Pixel super-resolution of time-stretch imaging by an equivalent-time sampling concept

Antony C. S. Chan, Edmund Y. Lam and Kevin K. Tsia

Department of Electrical and Electronic Engineering, the University of Hong Kong, Pokfulam, Hong Kong

ABSTRACT

Optical time-stretch imaging entails a stringent requirement of state-of-the-art high-speed data acquisition unit in order to preserve high image resolution at an ultrahigh frame rate — hampering the widespread application of such technology. We here propose a pixel super-resolution (pixel SR) technique tailored for time-stretch imaging that can relax the sampling rate requirement. It harnesses a concept of equivalent-time sampling, which effectively introduces sub-pixel shifts between frames. It involves no active opto-mechanical subpixel-shift control and any additional hardware. We present the system design rules and a proof-of-principle experiment which restores high-resolution images at a relaxed sampling rate of $5\,\mathrm{GSa/s}$.

1. INTRODUCTION

Optical time-stretch imaging relies on conversion of spectrally-encoded spatial information to the serial temporal waveform by group velocity dispersion.[1–3] Limited to the optical attenuation, the space-to-time conversion is generally limited to $0.05\,\mathrm{ns}/\mu\mathrm{m}$ or less. This implies that a state-of-the-art digitizer operating at over $20\,\mathrm{GSa/s}$ is required to resolve the micrometer-scale features for ultrafast microscopy applications. The acquired image is thus easily corrupted by aliasing if sampled at a lower rate.

However, the loss of high resolution can be restored by employing pixel super-resolution (pixel SR) algorithm from multiple subpixel-shifted, low-resolution images.[4,5] Previously, we demonstrated that real time sub-pixel shift can be realized by active control of beam deflection with acousto-optic beam deflector (AOD).[6] However, precise subpixel shifting in optical time-stretch imaging can be passively realized when the digitizer sampling clock is unlocked from the repetition rate of the laser — a feature common to many time-stretch imaging systems. By harnessing this effect at a slower sampling rate, we extract multiple low-resolution line-scans, each of which is introduced with a subpixel shift automatically. This technique resembles the concept of equivalent-time sampling adopted in sampling oscilloscope.[7,8] Unlike any classical pixel SR imaging techniques, this method requires no additional hardware for active subpixel-shift control. We here present the general system design rules and the algorithm for realizing pixel SR time-stretch imaging. We also show a proof-of-concept experiment with adaptive subpixel-registration and image restoration algorithms. At a lower sampling rate ($5\,\mathrm{GSa/s}$), we are able to restore the imaged feature size of $\sim 2\,\mu\mathrm{m}$ from the original aliased image with a pixel size of $3.6\,\mu\mathrm{m}$. We also demonstrate that such technique facilitates the morphological classification of phytoplankton culture.

2. THEORY

In the spectral-encoding imaging flow cytometry setup (Fig. 1A), the microfluidic channel is illuminated by a spectrally encoded pulsed laser beam. As the biological cells flow along the microfluidic channel, the pulsed laser beam captures a sequence of line-scans across the cell. The time-stretch spectrum analyzer then records and digitizes the captured sequence in real time. The two-dimensional image of the cell thus can be restored by stacking multiple line scans from the one-dimensional signal.

Owing to this special configuration, the dimensions of the image pixels are independent to each other. The pixel resolution along the flow direction is the product of linear flow rate (v_y) and the laser pulse repetition

Further author information: (Send correspondence to Kevin K. Tsia)
E-mail: tsia@hku.hk

High-Speed Biomedical Imaging and Spectroscopy: Toward Big Data Instrumentation and Management
edited by Kevin K. Tsia, Keisuke Goda, Proc. of SPIE Vol. 9720, 972004 · © 2015 SPIE
CCC code: 0277-786X/15/$18 · doi: 10.1117/12.2212034

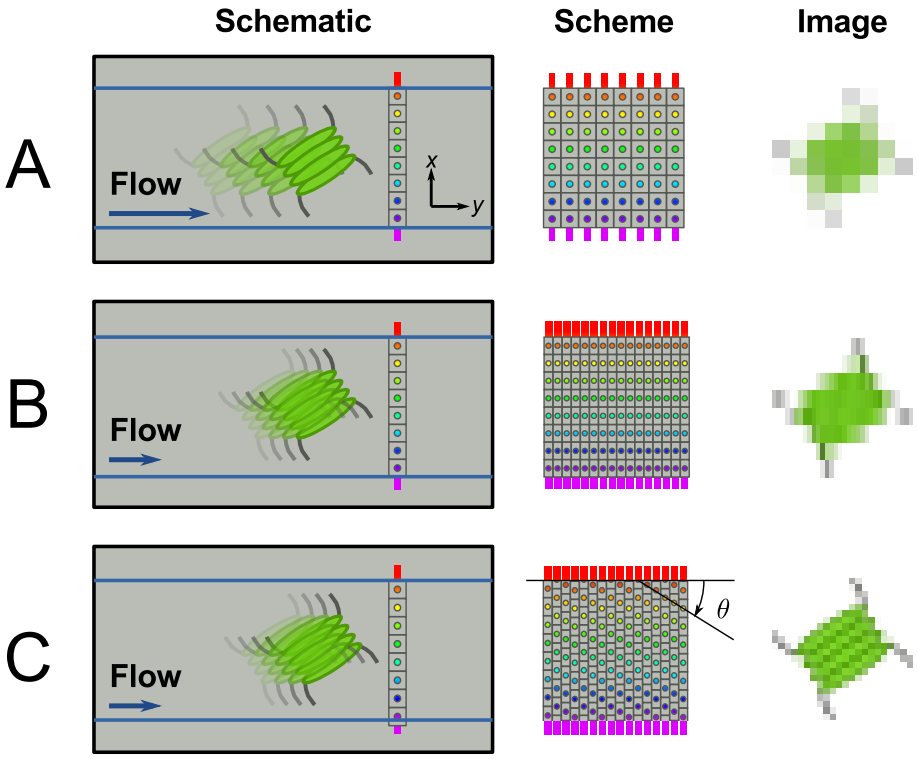

Figure 1. Over-sampling scheme of our method. (a) When the digitizer clock is locked to the laser pulse, the line scans are aligned to the microfluidic channel wall. Thus at low sampling rate, the cell sample appears as a highly pixelated image. (b) Pixel density along the flow direction can be increased by reducing the flow speed. (c) Asychronized sampling introduces sub-pixel shifts in consecutive line-scans, which improves pixel density orthogonal to the flow direction. The resultant pixel grid warping angle is denoted at θ.

rate (F), i.e. $\Delta y = v_y F$. Without changing hardware, it can be improved by reducing the flow rate (Fig. 1B). However, this has no effect on the pixel resolution perpendicular to the flow, which is independently determined by the resolving power of the microscopy setup and the time-strech spectrum analyzer, i.e.

$$\Delta x = \frac{C_x}{C_t f}, \tag{1}$$

where C_x is the wavelength-to-space conversion factor of the spectral encoding setup; C_t is the wavelength-to-time conversion factor of the time-stretch spectrum analyzer; and f is the sampling rate of the digitizer. Adjusting these three parameters involves hardware upgrade which is prohibitively expensive.

As mentioned in the introduction, pixel SR offers a way to improve Δx by taking advantage of line-by-line pixel drifting. Pixel drifting is observed when the digitizer clock is unlocked from the laser pulse, i.e. the sampling frequency f is not exactly the multiple of the laser pulse repetition rate F. In this case, the relative sub-pixel drift is given as

$$\delta x = \frac{C_x}{C_t} \times \left(\frac{1}{F} - N \times \frac{1}{f} \right), \quad |\delta x| \leq \Delta x/2, \tag{2}$$

where the integer N is the number of pixels per line scan. As shown in Fig. 1C, this results in warping of the pixel grid at a warp angle $\theta = \tan^{-1}(\delta x / \Delta y)$. For a large warp angle ($|\theta| \geq \pi/4$) and a very low linear flow rate ($\Delta y \ll \Delta x$), the transformed pixel resolution is given as

$$(\Delta x)' = \Delta x \cos\theta \leq \Delta x/\sqrt{2} \tag{3}$$

$$(\Delta y)' = \Delta y (\cos\theta)^{-1} \leq \sqrt{(\Delta y)^2 + (\Delta x/2)^2}. \tag{4}$$

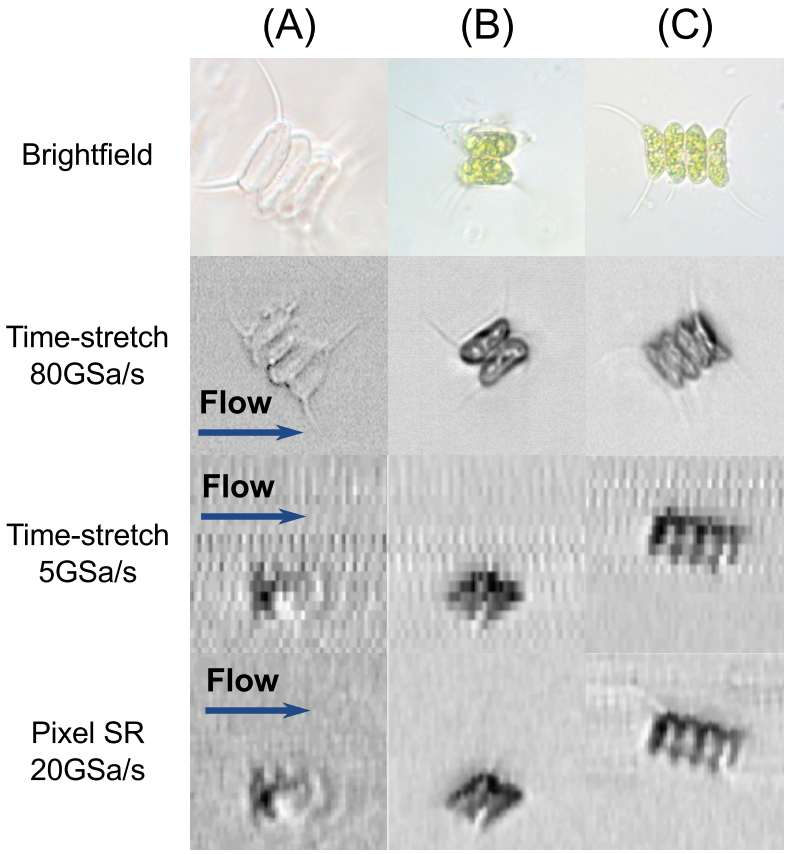

Figure 2. *Scendesmus* samples captured by the pixel SR time-stretch imaging: (a) discarded exoskeleton; (b) colony with two daughter cells; (c) colony with four daughter cells.

Here we see an improvement of $(\Delta x)'$ with a trade-off in $(\Delta y)'$. Note that this pixel drift does not increase the two-dimensional pixel density [i.e. $\Delta x \Delta y = (\Delta x)'(\Delta y)'$]. The increase in pixel density is purely due to the reduction of flow rate v_y.

3. EXPERIMENT AND RESULTS

We follow a unconventional flow cytometry protocol to classify cellular life stages solely based on the morphological phenotype. Compared to traditional fluorescence-stained approach, our technique does not require any labelling of the cells that could alter the cellular metabolism. To highlight the strength of pixel super-resolution to morphological classification, we choose a class of phytoplankton, *scenedesmus* (Carolina Biological, USA), for its distinct morphological property. *Scenedesmus* is a colony of either two or four daughter cells surrounded by the cell wall of the mother. Each daughter cell possesses an elongated shape at around $5\,\mu\mathrm{m}$ in diameter along the minor-axis[9] (first row, Fig. 2). At highest possible sampling rate ($80\,\mathrm{GSa/s}$), the cellular images comes with sharp outline and visible intracellular content (second row, Fig. 2). At a sample rate of $5/GSas$, however, the cell samples becomes highly aliased (third row, Fig. 2). Therefore, this specimen can serve as a resolution target to test resolution enhancement beyond $\Delta x \sim 2\,\mu\mathrm{m}$.

To highlight the strength of imaging flow cytometry enabled by optical time-stretch and pixel SR, we pass a population of around 1200 units of *Scendesmus* through a microfluidic channel at a linear speed of $1.6m/s$, and scan the cells at a laser repetition rate of $F = (11.6142 \pm 0.0005)\,\mathrm{MHz}$. The wavelength-to-time conversion factor $C_t = 0.40\,\mathrm{ns/\,nm}$ and the wavelength-to-space conversion factor of $C_x = 7.1\,\mu\mathrm{m/\,nm}$ are kept constant throughout the experiment. Without changing hardware, the sampling rate of the digitizer (Keysight technologies, USA) is down-adjusted from $80\,\mathrm{GSa/s}$ to $F = 5\,\mathrm{GSa/s}$. Hence, the apparent pixel dimensions are respectively $(\Delta x, \Delta y) = (3.6\,\mu\mathrm{m}, 0.18\,\mu\mathrm{m})$. By unlocking the sample clock from the laser pulse frequency, we can achieve a

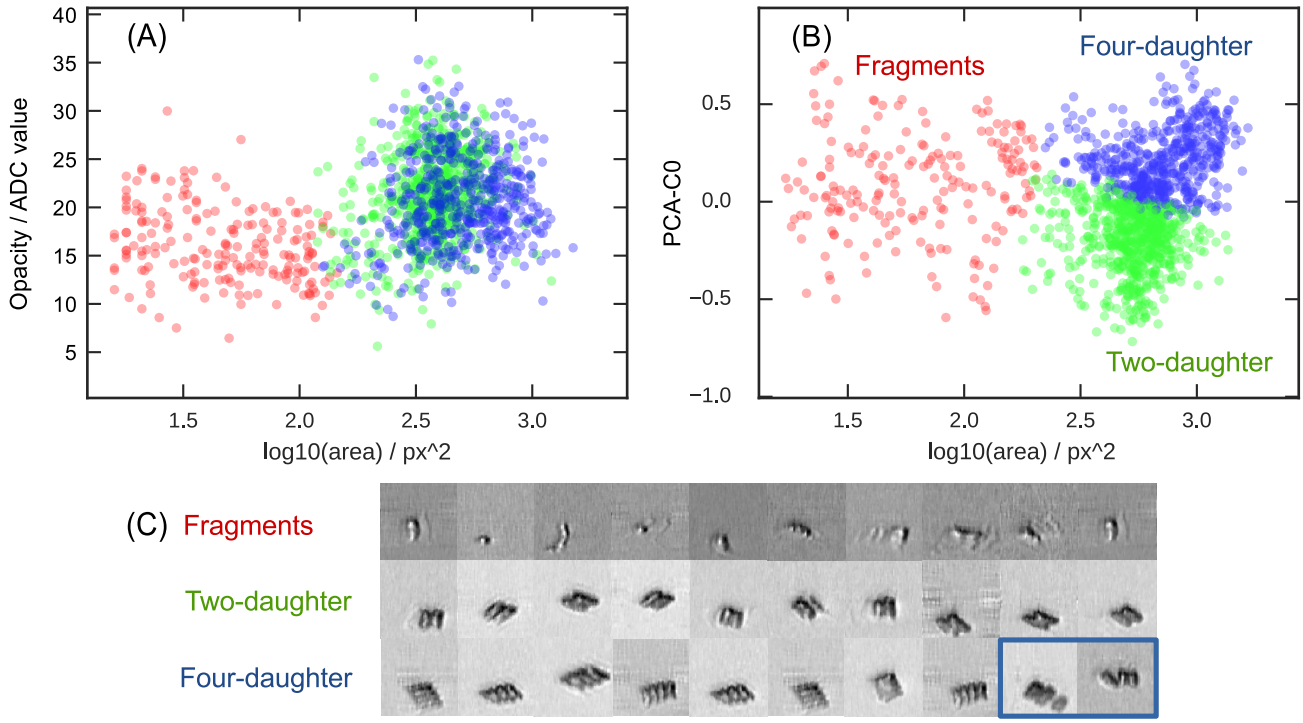

Figure 3. Classification of cell samples based on (A) mass and volume; (B) morphology and volume. (C) Examples of cell samples in corresponding groups. (Bottom right, highlighted) The aggregates of smaller colonies are mis-classified as four-daughter colony, but is clearly distinguishable in pixel SR time-stretch imaging.

pixel size far smaller than Δx. From Eq. 2, the relative pixel drifting is know to be roughly $\delta x = -1.8\,\mu\mathrm{m}$. The precise value of pixel grid warp angle θ is further refined by computational optimization. This step is essential for accurate pixel registration.[10] Subsequently, the warped grid is interpolated to a regular rectangular grid at a pixel dimensions of $0.9\,\mu\mathrm{m} \times 0.9\,\mu\mathrm{m}$, which is equivalent to a flow rate $v_y' = 8\,\mathrm{m/s}$ and a sample rate $F' = 20\,\mathrm{GSa/s}$. A matched filter is applied to suppress the noise amplified by the interpolation process. Refer to Appendix A for detailed computation steps.

To highlight the necessity of classification of unlabelled cell by morphology, we first attempt to group the cells in terms of cell mass and volume. These metrics are represented by cell opacity and area respectively, both measured from every cellular image captured from the experiment (Fig. 3A). Similar to forward scattering values obtained from traditional flow cytometry protocol, the above metrics failed to account for the morphological differences among the cell samples. In the case of *scendesmus*, only cell fragments can be distinguished from the scatter plot because they are significantly smaller and more translucent. In contrast, both two-daughter and four-daughter colonies are very similar in both opacity and area, thus they result in overlapping clusters in the scatter plot.

Next, we encode the morphological features of each image into the histogram of oriented gradients (HoG),[11] which is then projected to the most significant component using principle component analysis (PCA). The new structural metric is plotted against cell area in Fig. 3B. Without human intervention, the cell samples are divided into three groups by K-means clustering. By inspection, the three groups are later known to be cell fragments, two-daughter colony, and four-daughter colony respectively (Fig. 3C). Notably, we further identify rare aggregates of smaller colonies that are mis-classified as four-daughter colonies, as highlighted in Fig. 3C. However, it truly demonstrates the imaging capability of pixel SR time-stretch imaging which provides rich morphological information *unique* to every cell sample at lower digitizer cost.

4. CONCLUSIONS

We propose pixel SR for time-stretch imaging based on an equivalent time sampling concept prevalent to high-end oscilloscope. The sub-pixel shift of consecutive line scans originates from mismatch of laser pulse repetition frequency and sampling frequency, which is shared by many time-stretch imaging system. The value of sub-pixel shift, essential to accurate pixel SR restoration, can be estimated at high precision by computational optimization algorithm. We demonstrate the strength of this method by enhancing pixel resolution of existing imaging flow cytometry setup without additional hardware. The digitizer sampling rate can be relaxed to $5\,\mathrm{GSa/s}$ (i.e. apparent pixel size $3.6\,\mu\mathrm{m}$) without affecting classification of phytoplankton sized at $5\,\mu\mathrm{m}$. This approach can open up new applications of time-stretch imaging where the cost-effectiveness of the hardware is of concern.

ACKNOWLEDGMENTS

We thank Anson Tang, Queenie Lai and Bob Chung for technical assistance and helpful discussions. This work is partially supported by grants from the Research Grant Council of the Hong Kong Special Administration Region, China (Project No. 17207715, 17207714, HKU 720112E), Innovation and Technology Support Programme (ITS/090/14), University Development Fund of HKU, and the National Natural Science Foundation of China (NSFC)/Research Grants Council (RGC) Joint Research Scheme (N_HKU714/13).

APPENDIX A. COMPUTATIONAL SCHEME FOR PIXEL SUPER-RESOLUTION OF TIME-STRETCH IMAGING

A.1 Equivalent sampling time registration

The performance of pixel SR is highly sensitive to errors in pixel registration. A rough estimation of pixel drifting δx can be obtained from the specification of the pulsed laser and the digitizer. However, its precise value can only be estimated adaptively because the lasing cavity is highly susceptible to temperature and mechanical variation. In our approach, we model the pixel registration problem as a background suppression problem. Compared to the moving cell sample, the laser spectrum is highly consistent from pulse to pulse, which appears as bands along y axis in the background of the captured raw image. Given a rough estimate of the value of pixel drifting (and thus the warp angle θ), the lasing spectrum can be obtained by taking average of all the aligned pulses, i.e.

$$I_B(x, \tan\theta) = \frac{1}{M\Delta y} \int_0^{M\Delta y} \mathrm{unwarp}\{I(x,y), \tan\theta\}\, dy, \tag{5}$$

where M is the number of line scans of the warped image $I(x,y)$. The error of the initial warp angle can be iteratively reduced by reducing the foreground residual. In other words, the warp angle can be obtained by minimizing the energy of the foreground, i.e.

$$\tan\hat{\theta} = \arg\min_{\tan\theta} \int_0^{N\Delta x} \int_0^{M\Delta y} \left[\mathrm{unwarp}\{I(x,y), \tan\theta\} - I_B(x, \tan\theta)\right]^2 dx\, dy \tag{6}$$

The accuracy of this pixel registration approach is fundamentally limited by the decorrelation distance of the laser spectrum, i.e. $\epsilon[\tan\theta] < C_x \delta\lambda/(M\Delta y)$.

A.2 Background suppression

The highly modulated laser spectrum $I_B(x)$ is also aliased and must be restored to suppress the illumination background. From the third row of Fig. 2, direct subtraction of rawdata from the low-resolution form of $I_B(x)$ leaves zebra strip like artifacts parallel to the flow direction. For effective suppression of background, the high-resolution form of illumination background $I_B(x)$ is restored by interleaving the first several line scans, in which the cell sample is absent. The background is then projected back to the rawdata for direct subtraction.

A.3 Weighted non-uniform interpolation

Super-resolution restoration of the foreground (cell sample) can be obtained in two stages: non-uniform interpolation and convolution with the matched filter of the digitizer. The purpose of the first step is to re-sample the scattered samples to the regular rectangular grid. The second step is performed to suppress the noise amplified by the interpolation stage. The matched filter is approximately an elongated Gaussian function, which is the convolution of the two dimensional point spread function (PSF) of the imaging setup, and the one dimensional impulse response of the antialiasing filter in the digitizer. For higher computational efficiency, the above two stages are performed at once by using the value of the matched filter as the weights in the interpolation process. That is, for an SR pixel at position (x_0, y_0), its pixel value is

$$I(x_0, y_0) = \sum_{d_i \leq r} w(x_i - x_0, y_i - y_0)\, I(x_i, y_i), \tag{7}$$

where $d = \sqrt{(x_i - x_0)^2 + (y_i - y_0)^2}$; $w(x, y)$ is the two-dimensional matched filter; and r is the effective radius of $w(x, y)$.

REFERENCES

[1] Lau, A. K. S., Wong, T. T. W., Ho, K. K. Y., Tang, M. T. H., Chan, A. C. S., Wei, X., Lam, E. Y., Shum, H. C., Wong, K. K. Y., and Tsia, K. K., "Interferometric time-stretch microscopy for ultrafast quantitative cellular and tissue imaging at $1\,\mu$m," *Journal of Biomedical Optics* **19**, 076001 (Jul 2014).

[2] Wong, T. T. W., Lau, A. K. S., Ho, K. K. Y., Tang, M. Y. H., Robles, J. D. F., Wei, X., Chan, A. C. S., Tang, A. H. L., Lam, E. Y., Wong, K. K. Y., Chan, G. C. F., Shum, H. C., and Tsia, K. K., "Asymmetric-detection time-stretch optical microscopy (ATOM) for ultrafast high-contrast cellular imaging in flow," *Scientific Reports* **4**, 5636 (Jan 2014).

[3] Goda, K., Tsia, K. K., and Jalali, B., "Serial time-encoded amplified imaging for real-time observation of fast dynamic phenomena," *Nature* **458**, 1145–9 (apr 2009).

[4] Wong, T. T. W., Qiu, Y., Lau, A. K. S., Xu, J., Chan, A. C. S., Wong, K. K. Y., and Tsia, K. K., "Cost-effective approaches for high-resolution bioimaging by time-stretched confocal microscopy at $1\,\mu$m," *Optics in Health Care and Biomedical Optics V* **8553**, 85531P (Dec. 2012).

[5] Wong, T. T. W., Chan, A., Wong, K. K. Y., and Tsia, K. K., "Pixel super-resolution in serial time-encoded amplified microscopy (STEAM)," *Conference on Lasers and Electro-Optics, Optical Society of America* , CTu3J.4 (2012).

[6] Chan, A. C., Lam, E. Y., and Tsia, K. K., "Pixel super-resolution in optical time-stretch microscopy using acousto-optic deflector," *Conference on Optics in the Life Sciences, Optical Society of America* , PW2A.7 (2015).

[7] Keysight Technologies, "What is the difference between an equivalent time sampling oscilloscope and a real-time oscilloscope?," (2015). Available from http://cp.literature.agilent.com/litweb/pdf/5989-8794EN.pdf.

[8] Tektronix, "Real-time versus equivalent-time sampling," (Jan. 2001). Available from http://www.tek.com/document/application-note/real-time-versus-equivalent-time-sampling.

[9] Griffiths, D. J., [*Microalgal Cell Cycles*], ch. The Cell Cycle in Scenedesmus, 43, Nova Science (2010).

[10] Park, S., Park, M., and Kang, M., "Super-resolution image reconstruction: a technical overview," *Signal Processing Magazine, IEEE* , 21–36 (2003).

[11] Dalal, N. and Triggs, B., "Histograms of oriented gradients for human detection," *Conference on Optics in Health Care and Biomedical Optics V, IEEE Computer Society* **1**, 886–93 (June 2005).